PAN
ARCHIVES OF ACOUSTICS
Vol. **45**, No. 1, pp. 77–84 (2020)
DOI: 10.24425/aoa.2020.132483

Research Paper

Radiation of Sound Waves by a Semi-Infinite Duct with Outer Lining and Perforated End

Burhan TIRYAKIOGLU

Department of Applied Mathematics
Marmara University
Istanbul, Turkey
e-mail: burhan.tiryakioglu@marmara.edu.tr

(*received October 7, 2019; accepted November 20, 2019*)

Radiation of sound waves from a semi-infinite cylindrical duct with perforated end whose outer wall is coated with acoustically absorbent material is investigated by using the Wiener-Hopf technique in conjunction with the mode matching technique. A semi-infinite duct with a perforated screen can be used as a model for many engineering applications, such as noise reduction in exhausts of automobile engines, in modern aircraft jet, and turbofan engines. In particular, we aim to find the effects of outer lining and perforated end to sound pressure level for the underlying problem by using the standard Wiener-Hopf and mode matching techniques. We also present some numerical illustrations by determining the sound pressure level for different parameters such as soft and rigid outer surface, with and without perforated end, etc. Such investigations are useful in the reduction of noise effects generated through variety of sources.

Keywords: Wiener-Hopf; mode matching; perforated end; duct; radiation.

1. Introduction

The radiation of sound waves along duct systems is an important topic in radiation theory and relevant to many applications including reduction of noise in exhaust systems, in modern aircraft jet, and turbofan engines, etc. For this reason, a rigorous analysis of such engineering problems is required. Levine and Schwinger (1948) were the first who considered the problem of sound radiation from a semi-infinite circular unflanged duct of infinitely thin hard walls. An analytical solution was obtained based on the Wiener-Hopf technique (Noble, 1958). The Wiener-Hopf technique was applied later in papers by Weinstein (1969), Snakowska *et al.* (2017), Tiryakioglu and Demir (2019), etc. The reduction of noise in duct systems is generally achieved by silencers. The most well known of such silencers are acoustically absorbent linings, which have been widely analysed in literature (Rawlins, 1978; Buyukaksoy, Polat, 1998; Rawlins, 2007; Rienstra, 2007; Tiryakioglu, Demir, 2019). Rawlins (1978), who considered the radiation of sound from an unflanged rigid cylindrical duct with an acoustically absorbing internal surface, proved the effectiveness of absorbing lining. Another method of reducing noise is to create additional sound absorption by using the perforated structures. Perforated panel, or plate, are commonly employed to reduce sound pressure levels across a broad range of applications including industrial installations and propulsion devices (Yang *et al.*, 2015; Wang *et al.*, 2017). The phenomenon of perforated screens has been investigated by the authors (Nilsson, Brander, 1980; Tiryakioglu, 2019). This consideration is important because perforated screens provide some facilities for analysing of sound radiation.

The aim of this study is to investigate the effects of outer duct lining and perforated end on the radiation of sound. The presence of both outer lining and perforated end makes the problem more complicated when it is compared with the rigid outer duct and open ended case, and necessitates to adopt a formulation different to the classical method employed in (Rawlins, 1978). The used method is essentially the same as described in (Buyukaksoy, Polat, 1998) and consists of expressing the total field in the duct in terms of normal waveguide modes and using the Fourier Transform elsewhere. In this study, an analytical solution is obtained

based on the Wiener-Hopf technique. By applying direct Fourier transform, the problem is reduced into the solution of a Wiener-Hopf equation. Then, numerical solution is obtained for various values of the problem parameters such as impedance, perforated end, etc. The effect of these parameters on the radiation phenomenon is presented graphically by using the Matlab programming.

Validation of the numerical results of the current problem is achieved by different problems in the literature and the results are found to be in good agreement with the numerical results of two different studies (Tiryakioglu, Demir, 2019; Tiryakioglu, 2019).

2. Problem statement

This geometry consists of a semi-infinite duct with perforated end. The duct walls are assumed to be infinitely thin and they occupy the regions $\{\rho > a, z \in (-\infty, \infty)\}$, $\{\rho < a, z \in (l, \infty)\}$, and $\{\rho < a, z \in (-\infty, l)\}$ (see Fig. 1). The inner surface of cylinder is assumed to be rigid while its outer surface is assumed to be lined with acoustically absorbent material. The liner impedance is characterised by β. From the symmetry of the geometry of the problem and of the incident wave, the total field is taken independent of θ everywhere in the circular cylindrical coordinate system (ρ, θ, z). We shall therefore introduce a scalar potential $u(\rho, z)$ which defines the acoustic pressure and velocity by $p = i\omega\rho_0 u$ and $v = \operatorname{grad} u$, respectively, where ρ_0 is the density of undisturbed medium. The time dependence is assumed to be $e^{-i\omega t}$ and suppressed through the paper, where ω is the angular frequency.

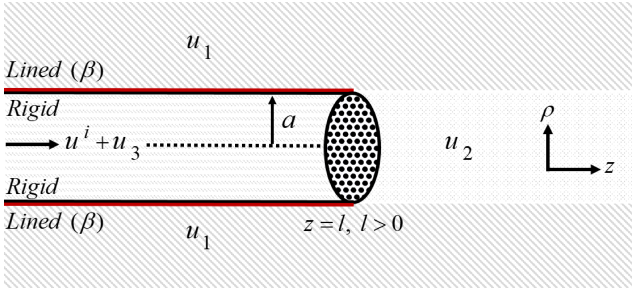

Fig. 1. Geometry of the problem.

Consider a time harmonic incident field propagating along a cylindrical waveguide with perforated end, as shown in Fig. 1, given by

$$u^i(z) = e^{ikz}. \tag{1}$$

Here $k = \omega/c$ denotes the wave number of the medium and c is the speed of sound. For the sake of analytical convenience, the total field (u^T) will be expressed as follows

$$u^T(\rho, z) = \begin{cases} u_1(\rho, z), & \rho > a, \ z \in (-\infty, \infty), \\ u_2(\rho, z), & \rho < a, \ z > l, \\ u_3(\rho, z) + u^i(z), & \rho < a, \ z < l, \end{cases} \tag{2}$$

where $u_1(\rho, z)$, $u_2(\rho, z)$, and $u_3(\rho, z)$ denote the unknown fields in their relevant regions. The field terms satisfy the below boundary conditions and continuity relations. The outer part is lined with an acoustically absorbent material having a surface impedance β, this gives

$$\left(ik\beta + \frac{\partial}{\partial\rho}\right) u_1(a_+, z) = 0, \quad z < l. \tag{3}$$

The boundary condition on the rigid surface can be given in terms of the potential function $u_3(\rho, z)$

$$\frac{\partial}{\partial\rho} u_3(a_-, z) = 0, \quad z < l. \tag{4}$$

Consider now the continuity conditions related to the total field at $\rho = a$, $z > l$ which are given by

$$\frac{\partial}{\partial\rho} u_1(a_+, z) = \frac{\partial}{\partial\rho} u_2(a_-, z), \quad z > l, \tag{5}$$

$$u_1(a_+, z) = u_2(a_-, z), \quad z > l. \tag{6}$$

From the continuity at the point $z = l$, $\rho < a$, we get

$$\frac{\partial}{\partial z} u_2(\rho, l) = \frac{\partial}{\partial z} u_3(\rho, l) + \frac{\partial}{\partial z} u^i(l), \quad \rho < a, \tag{7}$$

$$u_2(\rho, l) + i\frac{\zeta_p}{k}\frac{\partial}{\partial z} u_2(\rho, l) = u_3(\rho, l) + u^i(l), \quad \rho < a, \tag{8}$$

$$\zeta_p = [0.006 - ik(t_w + 0.75 d_h)]/\sigma, \tag{9}$$

where ζ_p is the specific impedance, describing the acoustic properties of the perforated screen. For stationary media, the empirical formula of the specific acoustic impedance ζ_p is given by Sullivan and Crocker (1978). Here, t_w is the screen thickness, d_h, the perforate hole diameter and σ, the porosity. Furthermore, to obtain a unique solution the following edge conditions at the mouth $\rho = a$, $z = l$ of the cylinder should be taken into account (Rawlins, 1978):

$$\frac{\partial}{\partial\rho} u_1 = \mathcal{O}(z^{-1/2}), \quad z \to l. \tag{10}$$

3. Derivation and solution of the Wiener-Hopf equation

In the region $\rho > a$, $z \in (-\infty, \infty)$ the unknown field $u_1(\rho, z)$ satisfies the Helmholtz equation

$$\left[\frac{1}{\rho}\frac{\partial}{\partial\rho}\left(\rho\frac{\partial}{\partial\rho}\right) + \frac{\partial^2}{\partial z^2} + k^2\right] u_1(\rho, z) = 0 \tag{11}$$

whose Fourier transform with respect to z yields

$$\left[\frac{1}{\rho}\frac{\partial}{\partial\rho}\left(\rho\frac{\partial}{\partial\rho}\right) + K^2(\alpha)\right] F(\rho, \alpha) = 0, \tag{12}$$

where $F(\rho, \alpha)$ stands for the Fourier transform of $u_1(\rho, z)$. Here, $K(\alpha) = \sqrt{k^2 - \alpha^2}$ is the square

root function defined in the complex α-plane (Tiryakioglu, Demir, 2019; Tiryakioglu, 2019)

$$F(\rho,\alpha) = \int_{-\infty}^{\infty} u_1(\rho,z)e^{i\alpha z}\,\mathrm{d}z = e^{i\alpha l}\left(F^-(\rho,\alpha)+F^+(\rho,\alpha)\right) \tag{13}$$

with

$$F^-(\rho,\alpha) = \int_{-\infty}^{l} u_1(\rho,z)e^{i\alpha(z-l)}\,\mathrm{d}z, \qquad F^+(\rho,\alpha) = \int_{l}^{\infty} u_1(\rho,z)e^{i\alpha(z-l)}\,\mathrm{d}z, \tag{14}$$

here $F^+(\rho,\alpha)$ and $F^-(\rho,\alpha)$ are analytic functions on upper region $\Im m\alpha > \Im m(-k)$ and lower region $\Im m\alpha < \Im mk$ of the complex α-plane, respectively. The general solution of (12) yields

$$e^{i\alpha l}\left(F^-(\rho,\alpha)+F^+(\rho,\alpha)\right) = A(\alpha)H_0^{(1)}(K\rho), \tag{15}$$

where $A(\alpha)$ is a spectral coefficient to be determined and $H_0^{(1)}$ is the Hankel function of the first type (Abramowitz, Stegun, 1964). Consider now the Fourier transform of (3), namely

$$e^{i\alpha l}\left(ik\beta F^-(a,\alpha)+\frac{\partial}{\partial\rho}F^-(a,\alpha)\right) = 0. \tag{16}$$

By taking the derivative of Eq. (15) with respect to ρ and using the relation given in (16), one can write

$$e^{i\alpha l}W^+(\alpha) = A(\alpha)H(\alpha), \tag{17}$$

where

$$W^+(\alpha) = ik\beta F^+(a,\alpha)+\frac{\partial}{\partial\rho}F^+(a,\alpha), \tag{18}$$

$$H(\alpha) = ik\beta H_0^{(1)}(Ka) - KH_1^{(1)}(Ka). \tag{19}$$

Substituting (17) into (15) yields

$$F^-(\rho,\alpha)+F^+(\rho,\alpha) = W^+(\alpha)\frac{H_0^{(1)}(K\rho)}{H(\alpha)}. \tag{20}$$

In the region $\rho < a$, $z > l$. The unknown field $u_2(\rho,z)$ satisfies the Helmholtz equation

$$\left[\frac{1}{\rho}\frac{\partial}{\partial\rho}\left(\rho\frac{\partial}{\partial\rho}\right)+\frac{\partial^2}{\partial z^2}+k^2\right]u_2(\rho,z) = 0 \tag{21}$$

whose Fourier transform is

$$\left[\frac{1}{\rho}\frac{\partial}{\partial\rho}\left(\rho\frac{\partial}{\partial\rho}\right)+K^2(\alpha)\right]G^+(\rho,\alpha) = f(\rho)-i\alpha g(\rho), \tag{22}$$

where $G^+(\rho,\alpha)$ is an analytic function in the upper α-plane, defined by

$$G^+(\rho,\alpha) = \int_{l}^{\infty} u_2(\rho,z)e^{i\alpha(z-l)}\,\mathrm{d}z, \tag{23}$$

while $f(\rho)$ and $g(\rho)$ stand for

$$f(\rho) = \frac{\partial}{\partial z}u_2(\rho,l), \qquad g(\rho) = u_2(\rho,l). \tag{24}$$

A particular solution of (22) can be expressed in terms of the Green's function related to this differential equation, which satisfies

$$\left[\frac{1}{\rho}\frac{\partial}{\partial\rho}\left(\rho\frac{\partial}{\partial\rho}\right)+K^2(\alpha)\right]\widetilde{G}(\rho,\rho',\alpha) = 0, \qquad \rho\neq\rho', \qquad \rho,\rho'\in(0,a) \tag{25}$$

with the condition that $\widetilde{G}(\rho,\rho',\alpha)$ must be limited at $\rho = 0$ as well as what follows:

$$\widetilde{G}(\rho'+0,\rho',\alpha)-\widetilde{G}(\rho'-0,\rho',\alpha) = 0, \qquad \frac{\partial}{\partial\rho}\widetilde{G}(\rho'+0,\rho',\alpha)-\frac{\partial}{\partial\rho}\widetilde{G}(\rho'-0,\rho',\alpha) = \frac{1}{\rho'}, \qquad \left(ik\beta+\frac{\partial}{\partial\rho}\right)\widetilde{G}(a,\rho',\alpha) = 0. \tag{26}$$

The solution is

$$\widetilde{G}(\rho,\rho',\alpha) = \frac{1}{J(\alpha)}Q(\rho,\rho',\alpha) \tag{27}$$

with

$$Q(\rho,\rho',\alpha) = \frac{\pi}{2}\begin{cases} J_0(K\rho)[J(\alpha)Y_0(K\rho')-Y(\alpha)J_0(K\rho')], & 0\le\rho\le\rho', \\ J_0(K\rho')[J(\alpha)Y_0(K\rho)-Y(\alpha)J_0(K\rho)], & \rho'\le\rho\le a, \end{cases} \tag{28}$$

where

$$J(\alpha) = ik\beta J_0(Ka) - KJ_1(Ka), \tag{29}$$

$$Y(\alpha) = ik\beta Y_0(Ka) - KY_1(Ka). \tag{30}$$

Here J_m and Y_m are the well known Bessel and Neumann functions of the order m. The solution of (22) can now be written as

$$G^+(\rho,\alpha) = \frac{1}{J(\alpha)}\left[B(\alpha)J_0(K\rho) + \int_0^a \left(f(t)-i\alpha g(t)\right)Q(t,\rho,\alpha)t\,\mathrm{d}t\right]. \tag{31}$$

Here $B(\alpha)$ stands for the spectral coefficient to be determined. Taking into account the continuity relation (5) and (6), one gets

$$B(\alpha) = W^+(\alpha). \tag{32}$$

Inserting now (32) into (31) we get

$$G^+(\rho,\alpha) = \frac{1}{J(\alpha)}\Bigg[W^+(\alpha)J_0(K\rho) + \int_0^a (f(t)-i\alpha g(t))\,Q(t,\rho,\alpha)t\,\mathrm{d}t\Bigg]. \quad (33)$$

The function $G^+(\rho,\alpha)$ is an analytic function on the upper half plane, but the zeros of $J(\alpha)$ on this half of complex α-plane violate the regularity of $G^+(\rho,\alpha)$. So, equating the residuals to zero at these poles, namely, at $\alpha=\alpha_m$:

$$ika\beta J_0(\gamma_m)-\gamma_m J_1(\gamma_m)=0,\quad \alpha_m=\sqrt{k^2-(\gamma_m/a)^2},\quad \Im m\alpha_m \geq \Im mk. \quad (34)$$

For the right hand side of (33) to be also analytic at $\alpha=\alpha_m$, we can derive

$$W^+(\alpha_m)=\frac{a}{2}J_0(\gamma_m)\left[1-(\beta ka/\gamma_m)^2\right][f_m-i\alpha_m g_m] \quad (35)$$

with

$$\begin{bmatrix} f_m \\ g_m \end{bmatrix} = \frac{2}{a^2 J_0^2(\gamma_m)\left[1-(\beta ka/\gamma_m)^2\right]} \cdot \int_0^a \begin{bmatrix} f(\rho) \\ g(\rho) \end{bmatrix} J_0\left(\frac{\gamma_m}{a}\rho\right)\rho\,\mathrm{d}\rho. \quad (36)$$

By using the continuity relation in (6) and considering the Eqs (20)–(33) we obtain

$$\frac{W^+(\alpha)}{M(\alpha)}-\frac{a}{2}F^-(a,\alpha) = -\frac{1}{2J(\alpha)}\int_0^a (f(\rho)-i\alpha g(\rho)) \cdot J_0(K\rho)\rho\,\mathrm{d}\rho, \quad (37)$$

where

$$M(\alpha)=\pi i J(\alpha)H(\alpha). \quad (38)$$

Owing to Eq. (36), $f(\rho)$ and $g(\rho)$ can be expanded into Dini series as follows (Watson, 1944)

$$f(\rho)=\sum_{m=1}^{\infty} f_m J_0\left(\frac{\gamma_m}{a}\rho\right),\qquad g(\rho)=\sum_{m=1}^{\infty} g_m J_0\left(\frac{\gamma_m}{a}\rho\right). \quad (39)$$

Performing the evaluation of the integrals at the right hand side of (37), one obtains the following Wiener-Hopf equation valid in the strip $\Im m(-k)<\Im m\alpha<\Im mk$:

$$\frac{W^+(\alpha)}{M(\alpha)}-\frac{a}{2}F^-(a,\alpha)=\frac{a}{2}\sum_{m=1}^{\infty}\frac{J_0(\gamma_m)}{\alpha_m^2-\alpha^2}\left[f_m-i\alpha g_m\right]. \quad (40)$$

The important step to solve the equation is to factorise kernel function as (Mittra, Lee, 1971):

$$M(\alpha)=M_+(\alpha)M_-(\alpha), \quad (41)$$

where $M_+(\alpha)$ is analytic and free of zeros in the upper half plane. Following the similar method used in (Buyukaksoy, Polat, 1998; Tiryakioglu, Demir, 2019), we obtain split functions as

$$M_+(\alpha)=\sqrt{\pi i\left(ik\beta J_0(ka)-kJ_1(ka)\right)a^*} \cdot\exp\left\{i\frac{a\alpha}{\pi}\left[1-C+\log\left(\frac{2\pi}{ka}\right)+i\frac{\pi}{2}\right]-\frac{ika}{2}\right\} \cdot\exp\left(\frac{aK(\alpha)}{\pi}\log\left(\frac{\alpha+iK(\alpha)}{k}\right)+q(\alpha)\right) \cdot\prod_{m=1}^{\infty}\left(1+\frac{\alpha}{\alpha_m}\right)\exp\left(\frac{i\alpha a}{m\pi}\right), \quad (42)$$

where

$$a^*=\left(ik\beta H_0^{(1)}(ka)-kH_1^{(1)}(ka)\right)$$

here C is the Euler's constant given by $C=0.57721...$ and $q(\alpha)$ stands for

$$q(\alpha)=\frac{1}{\pi}P\int_0^{\infty}\left[1-\frac{2}{\pi x}\frac{x^2-(\beta ka)^2}{b^*}\right] \cdot\log\left(1+\frac{\alpha a}{\sqrt{(ka)^2-x^2}}\right)\mathrm{d}x \quad (43)$$

where

$$b^*=(i\beta kaJ_0(x)-xJ_1(x))^2+(i\beta kaY_0(x)-xY_1(x))^2$$

and

$$M_-(\alpha)=M_+(-\alpha). \quad (44)$$

In (43), P denotes the Cauchy principle value at the singularities $x=ka$. Note that when we let $|\alpha|\to\infty$ in their respective regions of regularity, we have

$$M_\pm(\alpha)=\left(\pm\alpha^{1/2}\right). \quad (45)$$

The solution of (40) can easily be obtained through the classical Wiener-Hopf procedure. The result is

$$\frac{W^+(\alpha)}{M_+(\alpha)}=\frac{a}{2}\sum_{m=1}^{\infty}\frac{J_0(\gamma_m)\left[f_m+i\alpha_m g_m\right]M_+(\alpha_m)}{2\alpha_m(\alpha+\alpha_m)}. \quad (46)$$

4. Determination of the expansion coefficients

Consider now the waveguide region $\rho<a$, $z<l$ where the total field can be expressed in terms of Dini series as

$$u_3(\rho,z)=\sum_{n=0}^{\infty}a_n e^{-i\sigma_n z}J_0\left(\frac{j_n}{a}\rho\right) \quad (47)$$

with

$$J_1(j_n) = 0, \quad \sigma_n = \sqrt{k^2 - (j_n/a)^2}, \quad \sigma_0 = k. \tag{48}$$

Consider now the continuity relation in (7), (8) and using (24), namely,

$$f(\rho) = \frac{\partial}{\partial z} u_2(\rho, l) = \frac{\partial}{\partial z} u_3(\rho, l) + \frac{\partial}{\partial z} u^i(l), \tag{49}$$

$$g(\rho) = u_2(\rho, l) = u_3(\rho, l) + u^i(l) - i\frac{\zeta_p}{k}\frac{\partial}{\partial z} u_2(\rho, l). \tag{50}$$

Inserting the series expansions of $f(\rho)$ and $g(\rho)$ given in (39) in (49) and (50), respectively, and using (47), we get

$$\sum_{m=1}^{\infty} f_m J_0\left(\frac{\gamma_m}{a}\rho\right) = -i\sum_{n=0}^{\infty} \sigma_n a_n e^{-i\sigma_n l} J_0\left(\frac{j_n}{a}\rho\right) + ike^{ikl}, \tag{51}$$

$$\sum_{m=1}^{\infty}\left(g_m + i\frac{\zeta_p}{k} f_m\right) J_0\left(\frac{\gamma_m}{a}\rho\right) = \sum_{n=1}^{\infty} a_n e^{-i\sigma_n l} J_0\left(\frac{j_n}{a}\rho\right) + e^{ikl}. \tag{52}$$

Multiplying both sides of (51) and (52 by $\rho J_0\left(\frac{j_s}{a}\rho\right)$ and integrating from 0 to a, we obtain

$$\sum_{m=1}^{\infty} \frac{J_0(\gamma_m)}{\gamma_m^2}\left[f_m(1-\zeta_p) + ikg_m\right] = \frac{e^{ikl}}{a\beta}, \quad n = 0, \tag{53}$$

$$\frac{2ka\beta}{\sigma_n J_0(j_n)} \sum_{m=1}^{\infty} \frac{J_0(\gamma_m)}{\gamma_m^2 - j_n^2}\left[f_m\left(1 - \frac{\sigma_n\zeta_p}{k}\right) + i\sigma_n g_m\right] = 0, \quad n = 1, 2, ... \tag{54}$$

By substituting $\alpha = \alpha_1, \alpha_2, \alpha_3, ...$ in (46) and using (35) one can obtain

$$\frac{J_0(\gamma_r)\left[1 - (\beta ka/\gamma_r)^2\right][f_r - i\alpha_r g_r]}{M_+(\alpha_r)} = \sum_{m=1}^{\infty} \frac{J_0(\gamma_m)\,[f_m + i\alpha_m g_m]\, M_+(\alpha_m)}{2\alpha_m(\alpha_r + \alpha_m)}. \tag{55}$$

Formulas (53), (54), and (55) are the required linear systems of algebraic equations which permit us to determine f_m and g_m.

5. Analysis of the field

In the present paper we limit ourselves to the $\rho > a$ for radiated field. The field $\rho < a$ was analysed by Snakowska (1992). The radiated field in the region $\rho > a$ can be obtained by taking the inverse Fourier transform of $F(\rho, \alpha)$. By using (15) and (17), we write

$$u_1(\rho, z) = \frac{1}{2\pi}\int_{\mathcal{L}} W^+(\alpha)\frac{H_0^{(1)}(K\rho)}{H(\alpha)} e^{-i\alpha(z-l)}\,\mathrm{d}\alpha, \tag{56}$$

where $\mathcal{L}$ is a straight line parallel to the real α-axis, lying in the strip $\Im m(-k) < \Im m\alpha < \Im mk$. Utilising the asymptotic expansion of $H_0^{(1)}(K\rho)$ as $k\rho \to \infty$

$$H_0^{(1)}(K\rho) = \sqrt{\frac{2}{\pi K\rho}} e^{iK\rho - i\pi/4}. \tag{57}$$

Equation (56) can be evaluated through the saddle point technique (Snakowska, Idczak, 2006)

$$u_1(\rho, z) \sim \frac{k}{i\pi}\frac{W^+(-k\cos\theta)}{H(-k\cos\theta)}\frac{e^{ikr}}{kr}. \tag{58}$$

Here r and θ are the spherical coordinates defined by

$$\rho = r\sin\theta, \qquad z - l = r\cos\theta. \tag{59}$$

6. Results

In this section, the numerical results based on the mathematical formulation of the proposed study are presented. All graphics are obtained by applying the Matlab programming. Graphics are produced for Sound Pressure Level (SPL), defined by

$$\mathrm{SPL} = 20\log_{10}\left|\frac{p}{2\cdot 10^{-5}}\right|,$$

where p is the amplitude of the acoustic pressure of the sound wave, with the observation angle θ changing from 0 to π. The far field values are plotted at a distance 46 m away from the duct edge (Demir, Rienstra, 2010). Some parameter values remain unchanged in all examples. They are given below:

density of un. med.	$\rho_o = 1.255$ kg/m^3,
speed of sound	$c = 340.17$ m/s,
far radius	$r = 46$ m,
duct radius	$a = 0.1$ m,
duct extension	$l = 0.1$ m,
screen thickness	$t_w = 0.00081$ m,
hole diameter	$d_h = 0.0249$ m,
porosity	$\sigma = 0.037$.

The surface impedance β^{-1} determines the ability of a surface to guide and support the surface waves. $\beta^{-1} = \beta_1 + i\beta_2$, where β_1 and β_2 correspond to the resistace and reactance, respectively. The surface is lossless when the real part of the lining is zero and the surface waves can propagate on it without attenuation. The surface is lossy and surface wave is attenuated when real part is greater than zero. The imaginary part of the lining can be positive or negative, then the surface is said to be capacitive or inductive, respectively (Hassan, Rawlins, 1999; Tiwana *et al.*, 2016). Parameter values for lining and perforated end are taken from the study of (Sullivan, Crocker, 1978; Tiryakioglu, 2019; Peake, Abrahams, 2020).

All the numerical results were derived by truncating the infinite series and the infinite systems of linear algebraic equations after the first N terms. Figure 2 shows the variation of the sound pressure level against the truncation number N. It is seen that the amplitude of the sound pressure level becomes insensitive to the increase of the truncation number after $N = 10$.

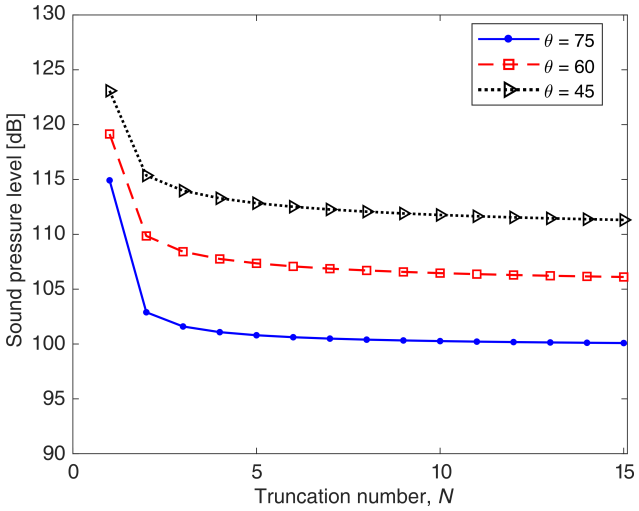

Fig. 2. Sound pressure level versus the truncation number N with $f = 2000$ Hz, $\beta^{-1} = 1 - 3i$.

Figure 3 displays the variation of the sound pressure level against the observation angle θ for values of $f = 1000$ Hz and $\beta^{-1} = 1 - 0.1i$, $\beta^{-1} = 1 - 1i$. As expected, the sound pressure level decreases with outer lining compared to the rigid surface.

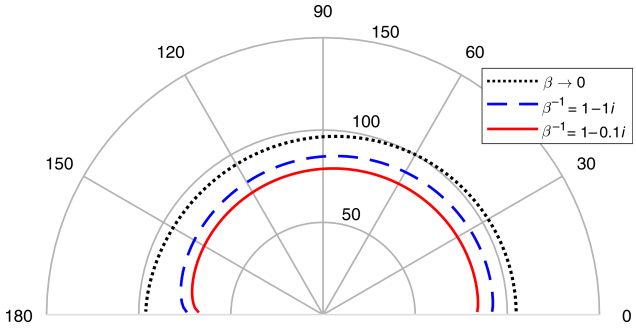

Fig. 3. Sound pressure level for rigid lined duct with $f = 1000$ Hz.

Figure 4 shows the variation of the sound pressure level versus observation angle for the values of different frequency. It is observed that the sound pressure level increases when the value of frequency is increased for $\beta^{-1} = 1 - 3i$.

Figures 5 and 6 display the variation of the sound pressure level for the values of reactance and resistance. As it can be seen, the sound pressure level can be reduced by changing the values of $\mathrm{Im}\,\beta^{-1}$ and $\mathrm{Re}\,\beta^{-1}$.

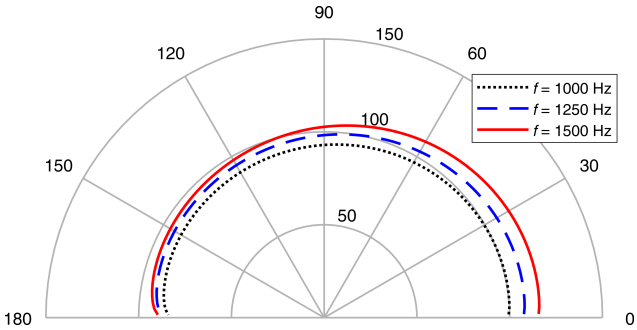

Fig. 4. Sound pressure level for different values of frequency with $\beta^{-1} = 1 - 3i$.

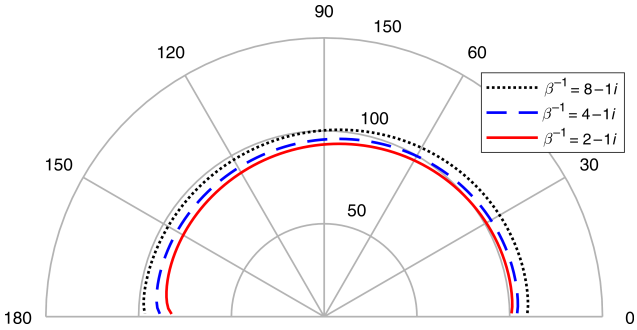

Fig. 5. Sound pressure level for different values of resistance with $f = 1250$ Hz.

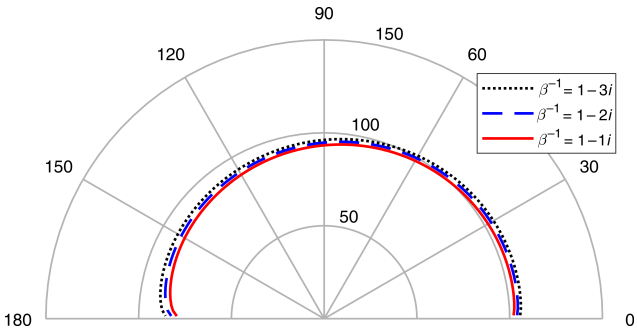

Fig. 6. Sound pressure level for different values of reactance with $f = 1250$ Hz.

Figures 7, 8, and 9 show the effect of the acoustic impedance of the perforated end on the sound pressure level with different values of frequencies and impedances. It is observed that perforated end provides additional sound absorbtion in all directions. Also, one can see that a second and third mode is revealed when the frequency is increased.

Figure 10 depicts the variation of the sound pressure level versus the outer surface impedance, which is taken purely imaginary (Demir *et al.*, 2002), for open perforated end duct with $f = 1000$ Hz. It is seen that sound pressure level decreases with $\beta_2 > 0$ compared to the $\beta_2 < 0$ case.

Figures 11 and 12 show an excellent agreement between the present paper and the study of (Tiryakioglu, Demir, 2019) and (Tiryakioglu,

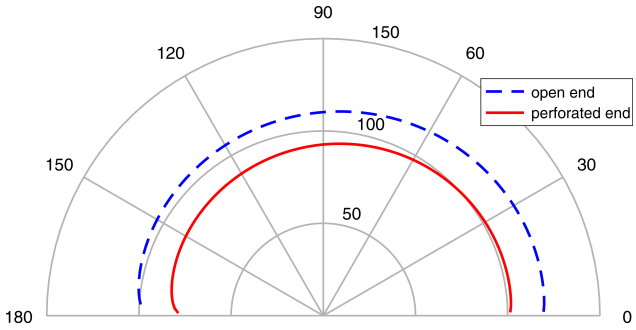

Fig. 7. Sound pressure level for open perforated end duct with $f = 1250$ Hz, $\beta^{-1} = 1 - 1i$.

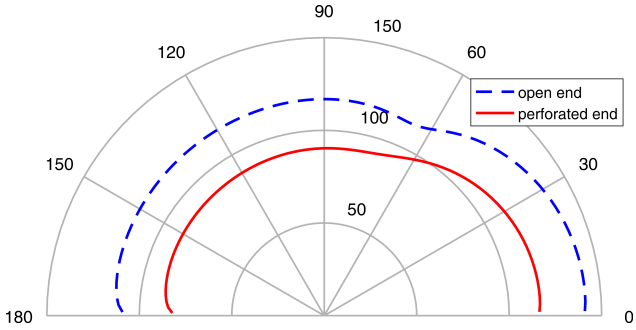

Fig. 8. Sound pressure level for open perforated end duct with $f = 2500$ Hz, $\beta^{-1} = 2 - 2i$.

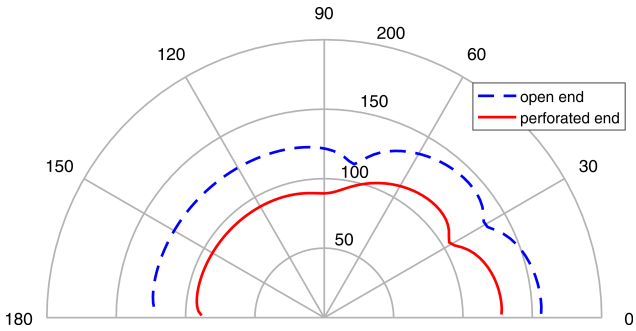

Fig. 9. Sound pressure level for open perforated end duct with $f = 4000$ Hz, $\beta^{-1} = 3 - 3i$.

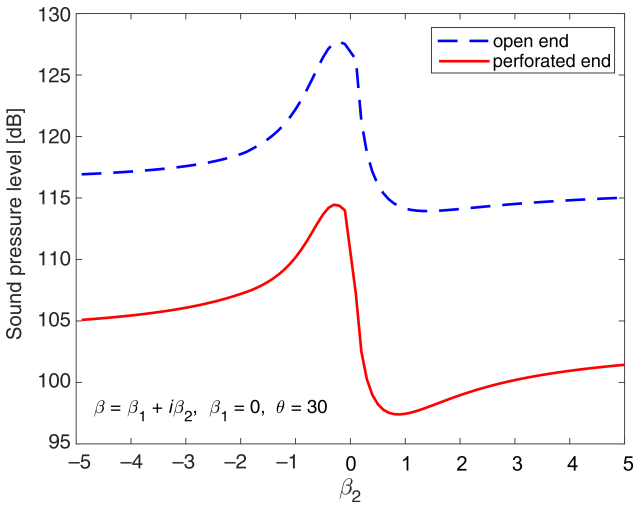

Fig. 10. Sound pressure level versus the surface impedance with $f = 1000$ Hz.

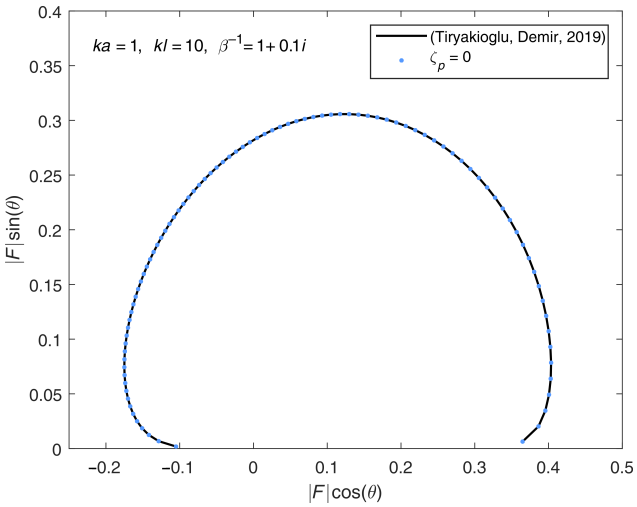

Fig. 11. Comparison of the radiated field with the study of (Tiryakioglu, Demir, 2019) with rigid inner surface.

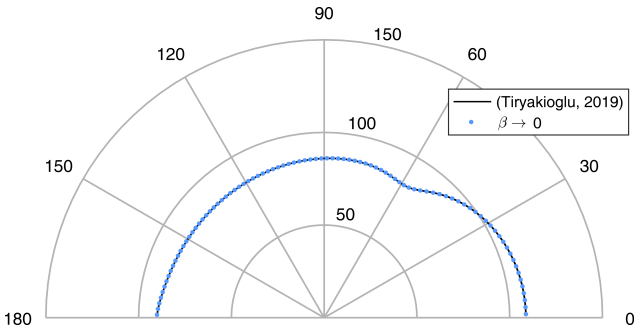

Fig. 12. Comparison of the sound pressure level with the study of (Tiryakioglu, 2019) with rigid outer surface.

2019), respectively, both in the radiated field and sound pressure level. In Fig. 11, when the perforated end is absent, the curve corresponding to $\zeta_p = 0$ coinsidse exactly with the result obtained in (Tiryakioglu, Demir, 2019) (Fig. 10, solid line). Notice that for Fig. 11,

$$\mathcal{F}(\theta) = \frac{k}{i\pi} \frac{W^+(-k\cos\theta)}{H(-k\cos\theta)}.$$

In Fig. 12, when the outer surface impedance approaches zero, the curve pertaining to sound pressure level agrees closely with the results of (Tiryakioglu, 2019) for the rigid pipe (Fig. 6, solid line).

7. Conclusions

The effect of the existence of outer lining and perforated end in the duct to the sound pressure level is investigated rigorously and some numerical results are presented. The problem is reduced to a Wiener-Hopf equation whose solution involves infinitely many expansion coefficients satisfying an infinite system of linear algebraic equations, solved by using the classical

factorisation and decomposition procedures. A numerical solution to these systems is obtained for various values of the problem parameters such as rigid lined cases, open perforated end, etc.

As it is well known, the inner absorbent lining provided a few decibels of sound wave reduction. In addition, it is found that presence of the outer lining and perforated end reduced the sound pressure level when compared with the rigid outer surface and open end case. In this case, by using both outer lining and perforated end, the highest sound absorption can be achieved.

The results are also compared with the study of (Tiryakioglu, Demir, 2019) (without perforated end) and (Tiryakioglu, 2019) (rigid duct). It is observed that the agreement is perfect.

References

1. Abramowitz M., Stegun I. (1964), *Handbook of mathematical functions*, Dover, New York.
2. Büyükaksoy A., Polat B. (1998), Diffraction of acoustic waves by a semi-infinite cylindrical impedance pipe of certain wall thickness, *Journal of Engineering Mathematics*, **33**: 333–352, doi: 10.1023/A:1004301829276.
3. Demir A., Büyükaksoy A., Polat B. (2002), Diffraction of plane sound waves by a rigid circular cylindrical cavity with an acoustically absorbing internal surface, *ZAMM – Journal of Applied Mathematics and Mechanics/Zeitschrift für Angewandte Mathematik und Mechanik*, **82**(9): 619–629, doi: 10.1002/1521-4001(200209)82:9<619::AID-ZAMM619>3.0.CO;2-E.
4. Demir A., Rienstra S. (2010), Sound radiation from a lined exhaust duct with lined afterbody, *16th AIAA/CEAS Aeroacoustics Conference*, 18 pages, Stockholm, Sweden, doi: 10.2514/6.2010-3947.
5. Hassan M., Rawlins A.D. (1999), Sound radiation in a planar trifurcated lined duct, *Wave Motion*, **29**(2): 157–174, doi: 10.1016/S0165-2125(98)00026-2.
6. Levine H., Schwinger J. (1948), On the radiation of sound from an unflanged circular pipe, *Physical Review*, **73**(4): 383–406, doi: 10.1103/PhysRev.73.383.
7. Mittra R., Lee S.W. (1971), *Analytical techniques in the theory of guided waves*, The Macmillan Company.
8. Nilsson B., Brander O. (1980), The propagation of sound in cylindrical ducts with mean flow and bulk-reacting lining. I. Modes in an infinite duct, *IMA Journal of Applied Mathematics*, **26**(3): 269–298, doi: 10.1093/imamat/26.3.269.
9. Noble B. (1958), *Methods based on the Wiener-Hopf techniques*, Pergamon Press, London.
10. Peake N., Abrahams I.D. (2020), Sound radiation from a semi-infinite lined duct, *Wave Motion*, **92**, doi: 10.1016/j.wavemoti.2019.102407.
11. Rawlins A.D. (1978), Radiation of sound from an unflanged rigid cylindrical duct with an acoustically absorbing internal surface, *Proceedings of the Royal Society of London. A. Mathematical and Physical Sciences*, **361**(1704): 65–91, doi: 10.1098/rspa.1978.0092.
12. Rawlins A.D. (2007), Wave propagation in a bifurcated impedance-lined cylindrical waveguide, *Journal of Engineering Mathematics*, **59**(4): 419–435, doi: 10.1007/s10665-007-9172-4.
13. Rienstra S.W. (2007), Acoustic scattering at a hard-soft lining transition in a flow duct, *Journal of Engineering Mathematics*, **59**(4): 451–475, doi: 10.1007/s10665-007-9193-z.
14. Snakowska A. (1992), The acoustic far field of an arbitrary Bessel mode radiating from a semi-infinite unflanged cylindrical wave-guide, *Acta Acustica United with Acustica*, **77**(2): 53–62.
15. Snakowska A., Idczak H. (2006), The saddle point method applied to selected problems of acoustics, *Archives of Acoustics*, **31**(1): 57–76.
16. Snakowska A., Jurkiewicz J., Gorazd L. (2017), A hybrid method for determination of the acoustic impedanceof an unflanged cylindrical duct for multimode wave, *Journal of Sound and Vibration*, **396**: 325–339, doi: 10.1016/j.jsv.2017.02.040.
17. Sullivan J.W., Crocker M.J. (1978), Analysis of concentric-tube resonators having unpartitioned cavities, *Journal of the Acoustical Society of America*, **64**(1): 207–215, doi: 10.1121/1.381963.
18. Tiryakioglu B. (2019), Sound radiation from the perforated end of a lined duct, *Acta Acustica united with Acustica*, **105**(4): 591–599, doi: 10.3813/AAA.919340.
19. Tiryakioglu B., Demir A. (2019), Radiation analysis of sound waves from semi-infinite coated pipe, *International Journal of Aeroacoustics*, **18**(1): 92–111, doi: 10.1177/1475472X18812802.
20. Tiryakioglu B., Demir A. (2019), Sound wave radiation from partially lined duct, *Archives of Acoustics*, **44**(2): 239–249, doi: 10.24425/aoa.2019.128487.
21. Tiwana M.H., Nawaz R., Mann A.B. (2016), Radiation of sound in a semi-infinite hard duct inserted axially into a larger infinite lined duct, *Analysis and Mathematical Physics*, **7**: 525–548, doi: 10.1007/s13324-016-0154-4.
22. Wang J., Rubini P., Qin Q. (2017), Application of a porous media model for the acoustic damping of perforated plate absorbers, *Applied Acoustics*, **127**: 324–335, doi: 10.1016/j.apacoust.2017.07.003.
23. Watson G.N. (1944), *Theory of Bessel functions*, Cambridge University Press, Cambridge.
24. Weinstein L.A. (1969), *The theory of diffraction and the factorization method*, Golem Press, Boulder, Colorado.
25. Yang C., Cheng L., Hu Z. (2015), Reducing interior noise in a cylinder using micro-perforated panels, *Applied Acoustics*, **95**: 50–56, doi: 10.1016/j.apacoust.2015.02.003.